Inorganic Chemistry

Article

pubs.acs.org/IC

Water Oxidation Catalysis with Nonheme Iron Complexes under Acidic and Basic Conditions: Homogeneous or Heterogeneous?

Dachao Hong,[†,∥] Sukanta Mandal,[‡,∥] Yusuke Yamada,[†] Yong-Min Lee,[‡] Wonwoo Nam,*[,‡] Antoni Llobet,*[,§,‡] and Shunichi Fukuzumi*[,†,‡]

[†]Department of Material and Life Science, Graduate School of Engineering, Osaka University, ALCA, Japan Science Technology Agency (JST), Suita, Osaka 565-0871, Japan

[‡]Department of Bioinspired Science, Ewha Womans University, Seoul 120-750, Korea

[§]Institute of Chemical Research of Catalonia (ICIQ), Avinguda Països Catalans 16, E-43007 Tarragona, Spain

Supporting Information

ABSTRACT: Thermal water oxidation by cerium(IV) ammonium nitrate (CAN) was catalyzed by nonheme iron complexes, such as Fe(BQEN)$(OTf)_2$ (**1**) and Fe(BQCN)-$(OTf)_2$ (**2**) (BQEN = *N*,*N*′-dimethyl-*N*,*N*′-bis(8-quinolyl)-ethane-1,2-diamine, BQCN = *N*,*N*′-dimethyl-*N*,*N*′-bis(8-quinolyl)cyclohexanediamine, OTf = $CF_3SO_3^-$) in a non-buffered aqueous solution; turnover numbers of 80 ± 10 and 20 ± 5 were obtained in the O_2 evolution reaction by **1** and **2**, respectively. The ligand dissociation of the iron complexes was observed under acidic conditions, and the dissociated ligands were oxidized by CAN to yield CO_2. We also observed that **1** was converted to an iron(IV)-oxo complex during the water oxidation in competition with the ligand oxidation. In addition, oxygen exchange between the iron(IV)-oxo complex and $H_2{}^{18}O$ was found to occur at a much faster rate than the oxygen evolution. These results indicate that the iron complexes act as the true homogeneous catalyst for water oxidation by CAN at low pHs. In contrast, light-driven water oxidation using $[Ru(bpy)_3]^{2+}$ (bpy = 2,2′-bipyridine) as a photosensitizer and $S_2O_8{}^{2-}$ as a sacrificial electron acceptor was catalyzed by iron hydroxide nanoparticles derived from the iron complexes under basic conditions as the result of the ligand dissociation. In a buffer solution (initial pH 9.0) formation of the iron hydroxide nanoparticles with a size of around 100 nm at the end of the reaction was monitored by dynamic light scattering (DLS) in situ and characterized by X-ray photoelectron spectra (XPS) and transmission electron microscope (TEM) measurements. We thus conclude that the water oxidation by CAN was catalyzed by short-lived homogeneous iron complexes under acidic conditions, whereas iron hydroxide nanoparticles derived from iron complexes act as a heterogeneous catalyst in the light-driven water oxidation reaction under basic conditions.

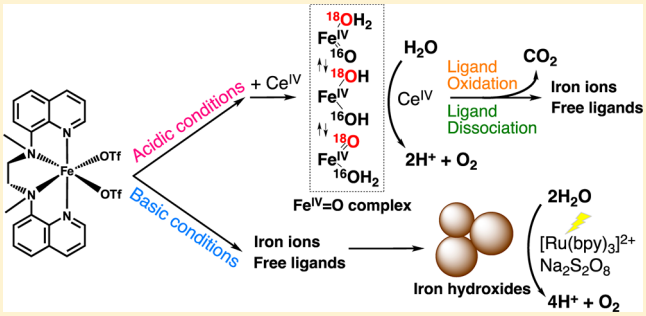

INTRODUCTION

One of the most promising candidates for a sustainable energy cycle is artificial photosynthesis that directly converts solar energy into chemical energy.[1−4] Artificial photosynthetic systems are composed of three functional parts, such as light-harvesting and charge-separation,[4] water oxidation,[5] and water reduction.[6] In these three parts, water oxidation is considered as the most challenging part because the process is an uphill energy transformation involving transfer of four electrons and four protons ($2H_2O \rightarrow O_2 + 4H^+ + 4e^-$).[7,8] Thus, extensive efforts have so far been devoted to developing homogeneous and heterogeneous water oxidation catalysts (WOCs).[9,10]

Many WOCs containing precious metals, such as ruthenium[11−16] and iridium,[17−20] have been reported to exhibit high activity in two major systems, such as thermal water oxidation by cerium(IV) ammonium nitrate (CAN) under acidic conditions and light-driven water oxidation under basic conditions using $[Ru(bpy)_3]^{2+}$ (bpy = 2,2′-bipyridine) and persulfate ($S_2O_8{}^{2-}$) as a photosensitizer and a sacrificial electron acceptor, respectively. For practical applications, the use of precious metals should be avoided because of its high cost and limited stock. Thus, much attention has been paid to the development of WOCs with earth-abundant metals such as cobalt,[21−24] copper,[25] manganese,[26−28] and iron.[29] Among these metals, iron is the most earth-abundant and environmentally benign metal often used as a catalyst in various oxidation reactions.[30,31] It has been reported recently that a series of homogeneous iron complexes with water coordination sites exhibit high catalytic activity for water oxidation by CAN with a maximum turnover value of 360.[32] Iron complexes have also been employed for light-driven water oxidation under basic conditions using $[Ru(bpy)_3]^{2+}$ and $S_2O_8{}^{2-}$ as a photosensitizer and a sacrificial electron acceptor, respectively.[33] In the light-

Received: May 11, 2013

   dx.doi.org/10.1021/ic401180r | Inorg. Chem. XXXX, XXX, XXX−XXX

driven water oxidation, iron complexes were converted to Fe_2O_3 as the true catalysts that conduct the water oxidation.[33] It has been suggested recently that the active iron catalysts for water oxidation at low and high pHs are different.[33] The oxidative degradation of ligands of metal complexes has been reported to produce metal oxide nanoparticles, which act as the true catalysts for water oxidation.[20,24,28] However, conditions to distinguish homogeneous iron complex catalysts versus heterogeneous iron catalysts derived from the iron complexes for the catalytic water oxidation have yet to be scrutinized.[34] The degradation of homogeneous iron complex catalysts due to the ligand oxidation during the catalytic water oxidation has also remained elusive. These issues on the homogeneous versus heterogeneous catalysis of iron-based materials as well as the water oxidation catalytic mechanism should be certainly clarified much more judging from the importance of the potential use of earth-abundant iron catalysts in water oxidation.

We report herein thermal and light-driven water oxidation reactions by employing two water-soluble mononuclear non-heme iron complexes, Fe(BQEN)$(OTf)_2$ (**1**) and Fe(BQCN)$(OTf)_2$ (**2**) (BQEN = *N*,*N*′-dimethyl-*N*,*N*′-bis(8-quinolyl)-ethane-1,2-diamine, BQCN = *N*,*N*′-dimethyl-*N*,*N*′-bis(8-quinolyl)cyclohexanediamine, OTf = $CF_3SO_3^-$) (Chart 1), to

Chart 1. Iron Complexes Used in Thermal and Light-Driven Water Oxidation Reactions

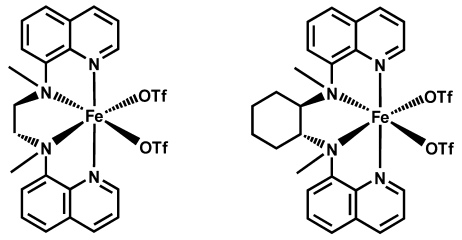

Fe(BQEN)$(OTf)_2$ (**1**) Fe(BQCN)$(OTf)_2$ (**2**)

disclose the true catalysts involved in those catalytic systems. Under acidic conditions, water oxidation by CAN was catalyzed by **1** and **2** in competition with the ligand oxidation. Under basic conditions, light-driven water oxidation by **1** showed the formation of iron hydroxide nanoparticles as the true catalyst. Thus, the true catalysts in the thermal and light-driven water oxidation reactions are shown to be different depending on pH conditions.

EXPERIMENTAL SECTION

Materials. All chemicals obtained from Aldrich Chemical Co. were the best available purity and used without further purification unless otherwise noted. Cerium(IV) ammonium nitrate (CAN), $Na_2S_2O_8$, and iron(II) sulfate were purchased from Wako Pure Chemical Industries Ltd. $H_2{}^{18}O$ (98% ^{18}O-enriched) was purchased from Taiyo Nippon Sanso Co. $[Ru(bpy)_3]Cl_2$ was obtained from Tokyo Chemical Industry Co., Ltd. $[Ru(bpy)_3]SO_4$ was synthesized by adding 1 equiv of Ag_2SO_4 to an aqueous solution of $[Ru(bpy)_3]Cl_2$. Purification of water (18.2 MΩ cm) was performed with a Milli-Q system (Millipore, Direct-Q 3 UV). $Fe(OTf)_2{\cdot}2CH_3CN$, Fe(BQEN)$(OTf)_2$ (**1**), and Fe(BQCN)$(OTf)_2$ (**2**) were synthesized according to the literature procedures.[35,36]

Oxygen Evolution Quantified by Manometry. Online manometric measurements were carried out on a Testo 521 differential pressure manometer with an operating range of 0.1−10 kPa and accuracy within 0.5% of the measurements. The manometer was coupled to thermostatic reaction vessels for dynamic monitoring of the headspace pressure above each reaction solution. The manometer's secondary ports were connected to thermostatic reaction vessels containing the same solvents and headspace volumes as the sample vials. Each measurement for a reaction solution (2.0 mL) was performed at 298 K.

Oxygen Evolution Quantified by GC. A vial (5.0 mL) containing an aqueous solution of an iron complex (1.0 mM or 12.5 μM, 2.0 mL) and another vial containing CAN (0.20 or 0.25 mmol) were sealed with a rubber septum. The two vials were carefully deaerated by bubbling Ar gas for 10 min. The aqueous solution of the iron complex (2.0 mL) in the vial was taken and injected into the vial containing CAN via a syringe piercing through the rubber septum to start the reaction with vigorous stirring. After each reaction time, 100 μL of Ar gas was injected into the vial, and then the same volume of gas in the headspace of the vial was sampled by a gastight syringe and quantified by a Shimadzu GC-17A gas chromatograph (GC) [Ar carrier, a capillary column with molecular sieves (Agilent Technologies, 19095PMS0, 30 m × 0.53 mm) at 313 K] equipped with a thermal conductivity detector (TCD).

The stoichiometric and repetitive experiments were performed as follows: An aqueous solution of CAN (0.20 M, 1.0 mL) containing HNO_3 (0.10 M) was prepared. An aliquot (40 μL) of the CAN solution (8.0 μmol) was injected to a nonbuffered aqueous solution of **1** (1.0 mM, 2.0 mL) in a vial deaerated by bubbling Ar gas to start the reaction (first run). Evolved oxygen gas in the headspace of the vial was quantified by GC. After 30 min, another aliquot (40 μL) of the CAN solution was injected to the solution of the first run deaerated again by bubbling Ar gas (second run), and the same procedure was applied for the third run.

Light-driven water oxidation was performed as follows: An iron complex (5.0 μM) was added to a borate buffer solution (100 mM, pH 8.0, 8.5 or 9.0, 2.0 mL) containing $Na_2S_2O_8$ (5.0 mM) and $[Ru(bpy)_3]SO_4$ (0.25 mM) deaerated by bubbling Ar gas. The solution was then irradiated with a xenon lamp (Ushio Optical, Model X SX-UID 500X AMQ) through a color filter glass (Asahi Spectra Co., Ltd.) transmitting $\lambda > 420$ nm at room temperature. Evolved oxygen gas in the headspace of the reaction vial was quantified by GC.

CO_2 Detection. Samples were prepared with the same procedures for the O_2 evolution measurements except for bubbling N_2 gas. After each reaction time, 50 μL of gas in the headspace was sampled and quantified by a Shimadzu GC-14B gas chromatograph (N_2 carrier, active carbon with a particle size of 60−80 mesh at 353 K) equipped with a TCD.

ESI-MS Measurements. Electrospray ionization mass spectra (ESI-MS) were collected on a Thermo Finnigan (San Jose, CA, U.S.A.) LCQTM Advantage MAX quadrupole ion trap instrument, by infusing samples directly into the source at 20 μL min^{-1} using a syringe pump. The spray voltage was set at 4.7 kV and the capillary temperature at 353 K.

^{18}O-Labeling Experiments. A volume of an aqueous solution (20 μL, $H_2{}^{16}O$) containing CAN (0.20 M) and HNO_3 (0.10 M) was injected into an aqueous solution (0.46 mL, $H_2{}^{16}O$) of **1** (2.0 μmol) in a vial (2.0 mL) deaerated by bubbling He gas for 20 min. A deaerated $H_2{}^{18}O$ solution (0.50 mL) was then added to the $H_2{}^{16}O$ solution followed by the additional injection of the CAN solution (20 μL, 4.0 μmol). After 10 min, 100 μL of gas in the headspace of the vial was sampled for gas analysis. The ratio of $^{16}O^{16}O$, $^{16}O^{18}O$, and $^{18}O^{18}O$ was determined based on the intensities of mass peaks (m/z = 32, 34, and 36) obtained by a Shimadzu GC-17A gas chromatograph [He carrier, a capillary column with molecular sieves (Agilent Technologies, 19095PMS0, 30 m × 0.53 mm) at 313 K] equipped with a Shimadzu QP-5000 mass spectrometer.

Spectroscopic Measurements. UV−vis absorption spectra were recorded on a Hewlett-Packard 8453 diode array spectrophotometer. Dynamic light scattering (DLS) measurements were performed with a Zetasizer Nano ZS instrument (Malvern Instruments Ltd., U.S.A.). The DLS instrument used in this study can detect the particle sizes ranging from 0.6 to 6000 nm.

dx.doi.org/10.1021/ic401180r | Inorg. Chem. XXXX, XXX, XXX−XXX

Electrochemical Measurements. Cyclic voltammetry (CV) and differential pulse voltammetry (DPV) measurements were performed on a CH Instruments 630B potentiostat using a glassy carbon electrode (3.0 mm diameter) as a working electrode, a saturated calomel electrode (SCE) as a reference electrode, and a Pt wire as an auxiliary electrode. Analyte concentrations (iron complexes or ligands) were 0.50 mM in water containing 0.10 M $NaNO_3$. The pH of a solution was adjusted using aqueous HNO_3 or NaOH solutions. All electrochemical measurements were carried out under nitrogen at room temperature with the scan rate of 100 mV s^{-1} for CV and amplitude of 50 mV and the pulse period of 0.2 s for DPV.

Characterization of Particles. Transmission electron microscope (TEM) images of nanoparticles, which were mounted on a copper micro grid coated with elastic carbon, were observed by a JEOL JEM 2100 operating at 200 keV. X-ray photoelectron spectra (XPS) were measured by a Kratos Axis 165x with a hemispherical electron energy analyzer. An incident radiation was Mg *Kα* X-ray (1253.6 eV) at 200 W, and a charge neutralizer was turned on for acquisition. Each sample was attached on a stainless stage with a double-sided carbon scotch tape. The binding energy of each element was corrected by the C 1s peak (284.6 eV) from the residual carbon.

RESULTS AND DISCUSSION

Water Oxidation by CAN Catalyzed by Iron Complexes. The catalytic water oxidation by CAN was investigated by adding an iron complex (12.5 μM) to an aqueous solution (2.0 mL) containing CAN (125 mM). The time courses of O_2 evolution quantified by gas chromatography (GC) are shown in Figure 1 (see GC charts in Supporting Information, Figure S1).

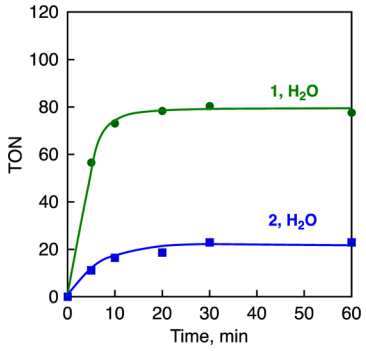

Figure 1. Time courses of O_2 evolution in the catalytic water oxidation by CAN (125 mM) with **1** and **2** (12.5 μM) in a nonbuffered aqueous solution (2.0 mL). O_2 was quantified by GC. TON is defined as the total number of moles of O_2 per mole of the complex.

When **1** and **2** were used as catalysts, O_2 evolution was observed with turnover numbers (TONs) of 80 ± 10 and 20 ± 5 at 60 min determined by GC. No O_2 evolution was observed in the absence of the iron complexes, indicating that the iron complexes catalyzed water oxidation. However, the O_2 yield in the reaction by **1** was less than 3.2% based on the stoichiometry of the reaction (eq 1),

$$2H_2O + 4Ce^{IV} \rightarrow O_2 + 4Ce^{III} + 4H^+ \quad (1)$$

in which one molecule of O_2 evolves from 4 equiv of CAN. The O_2 evolution was also quantified by manometry (Supporting Information, Figure S2); however, a slight amount of CO_2 was also evolved under the catalytic conditions (Supporting Information, Figure S3). Thus, TONs of O_2 evolution should be determined based on the direct detection of O_2 by GC together with the manometry.[32]

CAN is a strong oxidant ($E_{1/2}$ = 1.61 V vs. NHE),[37] and it has been reported to oxidize ligands of metal complexes and also to evolve CO_2 during the water oxidation reaction.[16,20,24,28] For this reason we analyzed the integrity of the BQEN ligand at the end of the water oxidation by CAN. ^{1}H NMR spectroscopy clearly demonstrated that the BQEN ligand was completely oxidized in the water oxidation reaction (Supporting Information, Figure S4). We also carried out CO_2 analysis by GC under the same conditions using a high concentration of iron complexes (1.0 mM). Figure 2 shows the time courses of

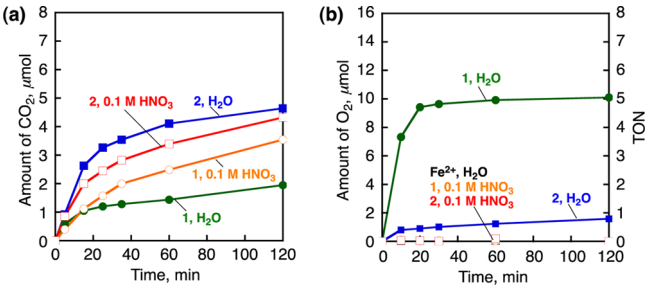

Figure 2. Time courses of (a) CO_2 evolution and (b) O_2 evolution in the catalytic water oxidation by CAN (0.10 M) with **1**, **2**, and $FeSO_4$ (1.0 mM) in a nonbuffered aqueous solution and in an aqueous solution containing 0.10 M HNO_3 (2.0 mL). The product yields were determined using GC.

CO_2 and O_2 evolution with **1**, **2**, and $FeSO_4$ performed in a nonbuffered aqueous solution and in an aqueous solution containing 0.10 M HNO_3. CO_2 evolution was observed with both **1** and **2** even at the initial reaction stage either in the nonbuffered solution or in the 0.10 M HNO_3 aqueous solution (Figure 2a, see GC charts in Supporting Information, Figure S5). This result clearly demonstrates that the ligands of **1** and **2** are completely degraded to CO_2 by CAN. The amount of CO_2 evolution observed with **2** (4.1 μmol) after 60 min is ~3 times larger than that observed with **1** (1.4 μmol), indicating BQCN ligand is more easily oxidized by CAN. The CO_2 evolution in the ligand oxidation of **1** and **2** competes with the O_2 evolution in the water oxidation by CAN. As shown in Figure 2b, O_2 evolution was also observed with **1** and **2** at the high concentration in the nonbuffered solution. The O_2 evolution with **1** was stopped at 20 min with a small TON of 5 and with an O_2 yield of 20% in the nonbuffered solution. The total amounts of O_2 and CO_2 evolution obtained with **1** agreed with the amount of evolved gas quantified by manometry (Supporting Information, Figure S6). The smaller amount of O_2 evolution with **2** could be ascribed to the larger amount of CO_2 evolution resulted from the ligand oxidation. The CO_2 evolution continued even after the O_2 evolution ceased in 20 min; this suggests that the deactivation of the WOC resulted from the ligand oxidation of the iron complexes by CAN.

When the reaction of **1** with CAN was performed in an aqueous solution in the presence of 0.10 M HNO_3, the amount of CO_2 evolution was twice larger than that in an aqueous solution without HNO_3 (Figure 2a). On the other hand, no O_2 evolution was observed with **1** and **2** in the presence of 0.10 M HNO_3 in water (Figure 2b). The ligand oxidation of **1** and **2** was accelerated, whereas the water oxidation was decelerated under highly acidic conditions. The ligands may be dissociated from iron complexes at low pHs to generate free iron ions, which have no catalytic activity for the water oxidation as no O_2

dx.doi.org/10.1021/ic401180r | Inorg. Chem. XXXX, XXX, XXX–XXX

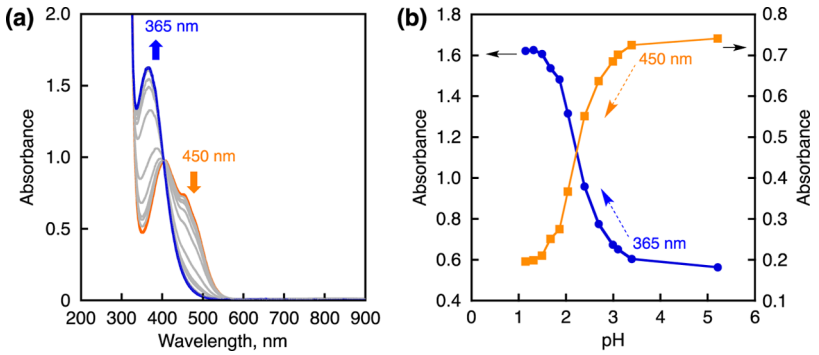

Figure 3. (a) UV−vis spectral changes by titration of nitric acid to a nonbuffered solution (2.0 mL) containing **1** (1.0 mM). (b) The absorbance changes at 450 and 365 nm observed with the titration.

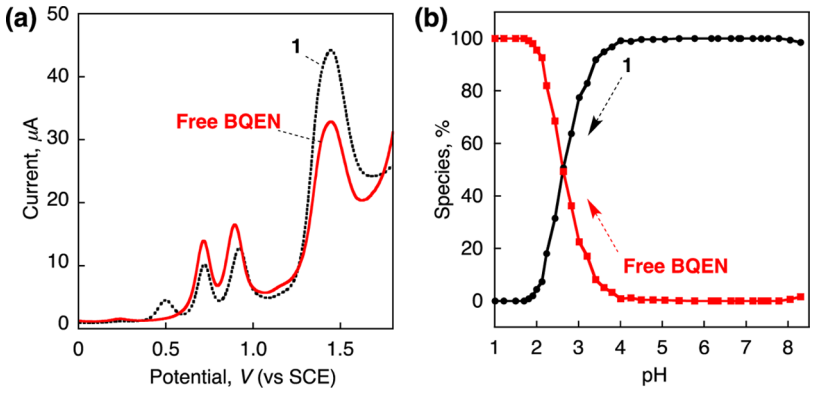

Figure 4. (a) Differential pulse voltammetry (DPV) of **1** (0.50 mM, black dotted line) or free BQEN ligand (0.50 mM, red line) in an aqueous solution (pH 2.4, 0.10 M $NaNO_3$). (b) pH dependence of distribution of **1** (black circles) and dissociated BQEN ligand (red square) determined by DPV measurements. The speciation curves were calculated by considering an equilibrium in aqueous medium: $Fe(BQEN)(OTf)_2 \rightleftharpoons$ "$Fe(OTf)_2$" + "BQEN" [% complex = {area of Fe^{III}/Fe^{II} curve/(area of Fe^{III}/Fe^{II} curve + area of first-step ligand oxidation curve)} × 100]. The areas of DPV curves were calculated by using software built in a CHI630b Electrochemical Analyzer. See Supporting Information, Figure S9 for DPV data obtained under different pH conditions.

evolution was observed from the reaction solution containing $FeSO_4$ (Figure 2b).

The ligand dissociation of **1** was examined with various concentrations of HNO_3 in an aqueous solution containing 1.0 mM of **1** as shown in Figure 3, where the absorption band at 450 nm due to **1** decreased with increasing concentration of HNO_3, accompanied by an increase in the absorption band at 365 nm due to free BQEN ligand (Supporting Information, Figure S7). The addition of NaOH to the resulting solution resulted in no recovery of the absorption band at 450 nm (Supporting Information, Figure S8). Thus, the ligand dissociation by HNO_3 is an irreversible process. The absorbance at 365 nm was plotted against the pH values together with the absorbance change at 450 nm as shown in Figure 3b. The BQEN ligand started to dissociate from **1** around pH 3.5 and completely dissociated at pH 1.5. This result explains why no O_2 was evolved with **1** in the presence of 0.10 M HNO_3 (Figure 2b).

The ligand dissociation of **1** at different pHs was also examined by differential pulse voltammetry in an aqueous solution containing **1** (0.50 mM) as shown in Figure 4 and Supporting Information, Figure S9. Under the acidic conditions (e.g., pH 2.4), the oxidation peaks due to both **1** and free BQEN ligand were observed (Figure 4a). The pH dependence on the ratio of the oxidation peaks due to **1** (~0.5 V vs SCE) and free BQEN ligand (~0.75 V) is shown in Figure 4b, which agrees with the absorbance changes depending on pH in Figure 3b. A cyclic voltammogram of **1** at pH 3.4, where the BQEN ligand is not dissociated significantly, exhibits the catalytic current for O_2 evolution in addition to the small oxidation peaks due to **1** and free BQEN ligand (Supporting Information, Figure S10).

The pH of a 0.10 M CAN aqueous solution was 0.80, which enabled the BQEN ligand to dissociate completely from **1** as shown in Figures 3b and 4b. However, O_2 was evolved in water oxidation by 0.10 M CAN with **1** in a nonbuffered aqueous solution (Figure 2b). This indicates that the catalytic water oxidation by CAN with **1** occurs in competition with the ligand dissociation of **1**. Indeed, the ligand dissociation by an acid was observed to occur within several seconds (Supporting Information, Figure S11); however, high-valent iron complexes formed in the presence of CAN prohibited the ligand dissociation because of the strong binding of the ligands to the high-valent metal center, which resulted from the strongly electron-withdrawing ability of the high-valent iron. The oxidation of **1** by CAN resulted in rapid production of a high-valent iron complex, which is continuously formed by excess CAN during the water oxidation (vide infra). The O_2 evolution was stopped at 20 min, since the ligand was completely dissociated from **1**. Thus, the use of a nonbuffered aqueous solution is important to achieve the catalytic water oxidation with **1** to evolve O_2, because the ligand was dissociated in a buffered acid solution before the addition of CAN.

dx.doi.org/10.1021/ic401180r | Inorg. Chem. XXXX, XXX, XXX−XXX

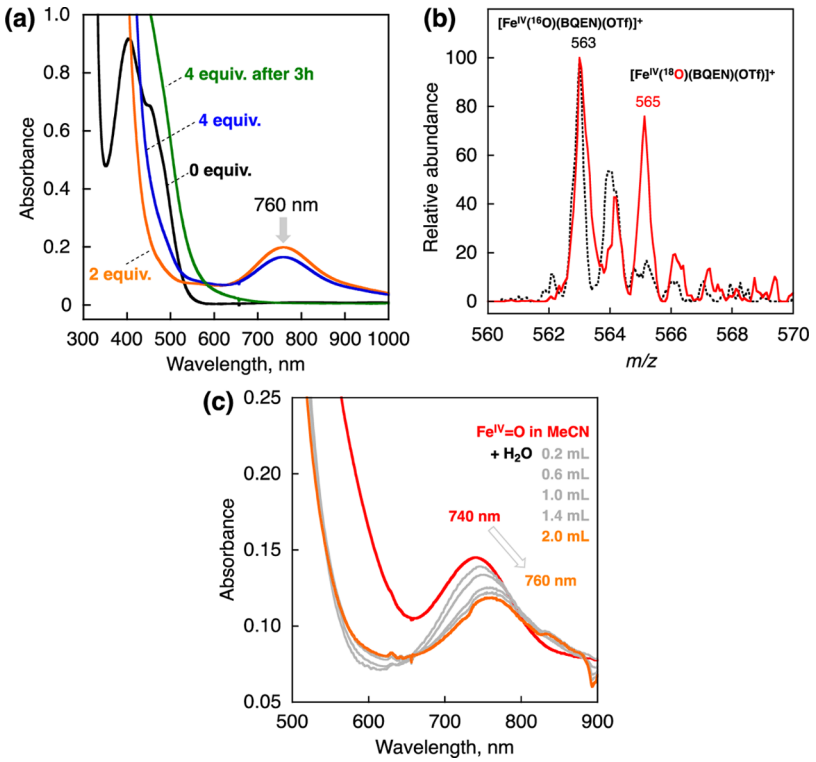

Figure 5. (a) UV−vis spectral changes observed in the stoichiometric water oxidation by **1** (1.0 mM) upon addition of different amounts of CAN (1.0−4.0 mM) in a nonbuffered aqueous solution (2.0 mL). (b) ESI-MS spectra of $[Fe^{IV}(BQEN)(O)(OTf)]^+$ formed in the reaction of **1** (1.0 mM) with peracetic acid (1.2 mM) in the presence of $H_2{}^{16}O$ (20 μL, black dots) and $H_2{}^{18}O$ (20 μL, red line) in MeCN (2.0 mL). The peaks at m/z 563.0 and 565.0 correspond to $[Fe^{IV}(BQEN)(^{16}O)(OTf)]^+$ and $[Fe^{IV}(BQEN)(^{18}O)(OTf)]^+$ (calcd m/z = 563.1 and 565.1, respectively). (c) UV−vis spectral changes of Fe^{IV}=O (1.0 mM, red line) upon addition of various amounts of H_2O (gray lines: 0.20 mL, 0.60 mL, 1.0 mL, 1.4 mL, and orange line: 2.0 mL) into an MeCN solution (2.0 mL) of Fe^{IV}=O at 273 K. The Fe^{IV}=O intermediate was generated in the reaction of **1** (1.0 mM) with peracetic acid (4.0 mM) in MeCN at 273 K.

DLS measurements were performed to examine the formation of nanoparticles during the O_2 evolution as shown in Supporting Information, Figure S12; no formation of nanoparticles was observed. Generally, particles of iron oxides are rarely derived from iron ions under acidic conditions at ambient temperature.[38]

Intermediates for Water Oxidation by 1 and CAN. The stoichiometric oxidation of **1** by CAN was investigated in a nonbuffered aqueous solution to detect the intermediate(s) formed in the catalytic water oxidation. When 2 equiv of CAN were added to the solution, an absorption band at 760 nm appeared (Figure 5a). The same absorption band was observed when excess CAN (0.10 M) was used (Supporting Information, Figure S13). The absorption band at 760 nm can be assigned to $[Fe^{IV}(BQEN)(O)]^{2+}$ (Fe^{IV}=O) by comparison with that of $[Fe^{IV}(BQEN)(O)]^{2+}$ prepared independently by the reported method, in which **1** was reacted with peracetic acid in MeCN.[39−41] The ESI-MS peak due to $[Fe^{IV}(BQEN)(^{16}O)(OTf)]^+$, which was produced by the reaction of **1** with peracetic acid in MeCN in the presence of $H_2{}^{16}O$, was observed at m/z = 563.0, which was shifted to m/z = 565.0 when the reaction was performed in MeCN in the presence of $H_2{}^{18}O$ (Figure 5b). The latter result is in line with our recent result that an intermediate containing oxygen atom exchanges its oxygen with $H_2{}^{18}O$ to produce $[Fe^{IV}(BQEN)(^{18}O)(OTf)]^2$.[40] The absorption band observed at 740 nm due to $[Fe^{IV}(BQEN)(O)]^{2+}$ in MeCN was shifted to 760 nm upon addition of H_2O (Figure 5c), probably because of the coordination of H_2O (vide infra) or protonation, in agreement with the absorption band observed in the oxidation of **1** by 2 equiv of CAN (Figure 5a).

To understand the role of Fe^{IV}=O in the catalytic water oxidation by CAN, the relation between O_2 evolution and the formation and decay of Fe^{IV}=O was investigated by comparing the time courses of the absorbance at 760 nm due to Fe^{IV}=O and O_2 evolution as shown in Figure 6. When 4 equiv of CAN were added to a nonbuffered aqueous solution of **1**, the absorption band at 760 nm assigned to Fe^{IV}=O immediately appeared, and decreased gradually as the O_2 evolution occurred and then ceased. The O_2 yield was determined to be 24% in the first run. Upon second and third addition of 4 equiv of CAN, the absorption band at 760 nm due to Fe^{IV}=O increased again immediately (Figure 6a), but each at initial absorbance was lower than that of previous run because of the ligand dissociation due to the gradually pH decrease in each time. The initial pH was 5.4 and decreased to 2.1, to 1.8, and then to 1.7 at the end of the first, second, and third runs, respectively. The yields of O_2 evolved at the second and third runs were 28% and 18%, respectively, which may be caused by two opposite factors, such as the higher oxidizing ability of CAN and increasing ligand dissociation at lower pH (Figures 3 and 4). The prohibition of the ligand dissociation from the iron complex was confirmed by the rapid formation of the Fe^{IV}=O complex, because the decay of absorbance at 760 nm due to Fe^{IV}=O was much slower than the ligand dissociation by the addition of an acid (Supporting Information, Figure S11). The formation of Fe^{IV}=O prevented ligand dissociation; however,

dx.doi.org/10.1021/ic401180r | Inorg. Chem. XXXX, XXX, XXX−XXX

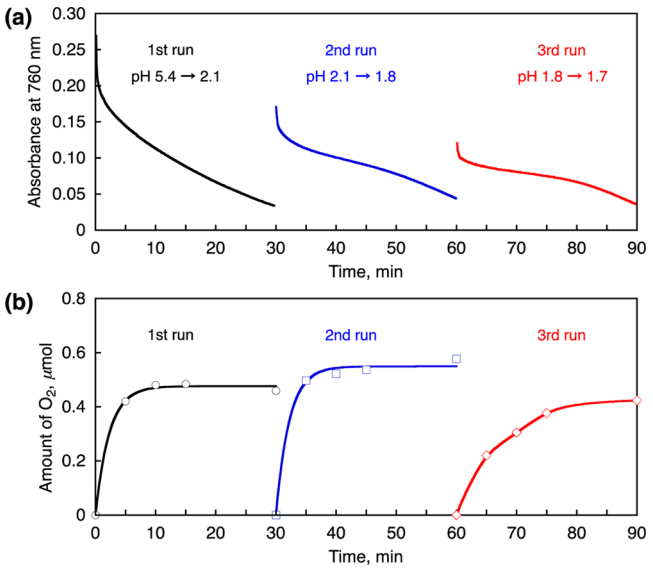

Figure 6. (a) Time courses of the absorbance at 760 nm in the water oxidation by addition of 4 equiv of CAN (4.0 mM) to **1** (1.0 mM) in a nonbuffered aqueous solution (2.0 mL, first run, black line), and further additions of CAN (4.0 mM) to the resulting solution for the second run (blue line), and the third run (red line). (b) Time courses of O_2 evolution quantified by GC in those reactions.

the Fe^{IV}=O decomposed during the reaction in a similar way to the decomposition of Fe^{II} complexes under acidic conditions.

When the stoichiometric reaction of CAN with **1** was performed in the presence of 0.10 M HNO_3 in water (pH 1.2), neither O_2 evolution nor the absorption band at 760 nm due to Fe^{IV}=O was observed because of the complete ligand dissociation from **1** (Supporting Information, Figure S15). These results indicate that the catalytic water oxidation by CAN with **1** occurs via formation of Fe^{IV}=O.

Mechanistic Insight into Water Oxidation by 1 and CAN. To gain mechanistic insight into the O−O bond formation in the catalytic water oxidation by CAN with **1**, the oxygen exchange in $[Fe^{IV}(BQEN)(^{16}O)]^{2+}$ with $H_2{}^{18}O$ (98% ^{18}O-enriched) was further examined by GC-MS (Figure 7). First the reaction of **1** with 2 equiv of CAN was performed in $H_2{}^{16}O$ to produce Fe^{IV}=^{16}O and then 2 equiv of CAN in $H_2{}^{18}O$ was added to the resulting solution to detect the isotopes of evolved O_2. The evolved O_2 was detected by GC-MS, which revealed that the isotope ratio of $^{16}O^{16}O$: $^{18}O^{16}O$: $^{18}O^{18}O$ was 27.3: 47.7: 25.0 (Figure 7), which agrees with the theoretical ratio (26.5: 50.0: 23.5) calculated by assuming that the oxygen exchange between $[Fe^{IV}(BQEN)(^{16}O)]^{2+}$ and $H_2{}^{18}O$ is much faster than the oxygen evolution under the reaction conditions. If the oxygen exchange between $[Fe^{IV}(BQEN)(^{16}O)]^{2+}$ and $H_2{}^{18}O$ is much slower than the oxygen evolution, no $^{18}O^{18}O$ would be evolved. Thus, the oxygen exchange between $[Fe^{IV}(BQEN)(^{16}O)]^{2+}$ and $H_2{}^{18}O$ (48.5%) occurs rapidly via $[Fe^{IV}(BQEN)(^{16}OH)(^{18}OH)]$ following coordination of $H_2{}^{18}O$ to produce the same amount of $[Fe^{IV}(BQEN)(^{16}O)]^{2+}$ and $[Fe^{IV}(BQEN)(^{18}O)]^{2+}$ as indicated in Figure 5b (Scheme 1b and c). Both $[Fe^{IV}(BQEN)(^{16}O)]^{2+}$ and $[Fe^{IV}(BQEN)(^{18}O)]^{2+}$ are further oxidized with CAN in $H_2{}^{16}O$ (51.5%) and $H_2{}^{18}O$ (48.5%) as solvent to produce O_2 with the theoretical isotope ratio of $^{16}O^{16}O$: $^{18}O^{16}O$: $^{18}O^{18}O$ = 26.5: 50.0: 23.5 (Scheme 1a−d).

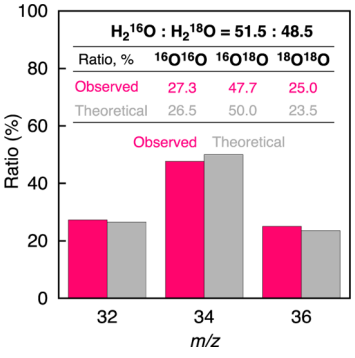

Figure 7. Comparison of relative abundance of ^{18}O-labeled and unlabeled oxygen evolved during the stoichiometric oxidation of $H_2{}^{18}O$-enriched water (48.5% $H_2{}^{18}O$) by addition of 2 equiv of CAN to **1** (2.0 μmol) in $H_2{}^{16}O$ followed by the addition of $H_2{}^{18}O$ and additional 2 equiv of CAN.

Scheme 1. Proposed Mechanism of Oxygen Exchange in $Fe^{IV}(^{16}O)$ with $H_2{}^{18}O$ in Relation with the Mechanism of the O−O Bond Formation in the Catalytic Water Oxidation by CAN with 1

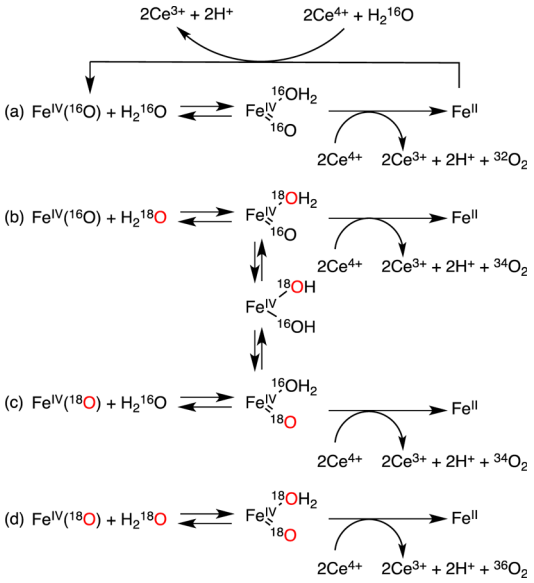

The formation of an O−O bond in $[Fe^{IV}(BQEN)(O)(OH_2)]^{2+}$ may be a key step, though it would be difficult to distinguish whether an O−O bond is formed by intramolecular interaction between the Fe^{IV}=O and Fe^{IV}−OH groups or the nucleophilic attack by water to Fe^{IV}=O from the labeling experiments. If H_2O_2 is produced from the O−O bond formation, it will be oxidized by 2 equiv of CAN to evolve O_2. Thus, we have investigated the H_2O_2 oxidation by CAN to confirm the rate-determining step in the water oxidation by CAN. When 2 equiv of CAN were added to H_2O_2 in an aqueous solution containing HNO_3 (0.10 M), the absorbance at 420 nm assigned to CAN completely disappeared within 20 s accompanied by O_2 evolution (Figure 8). The O_2 yield for the H_2O_2 oxidation reached 55% at 60 s and 90% at 300 s according to the stoichiometric reaction of eq 2. This result suggests that O_2 was evolved rapidly when H_2O_2 was oxidized by 2 equiv of CAN.

$$H_2O_2 + 2Ce^{IV} \rightarrow O_2 + 2Ce^{III} + 2H^+ \quad (2)$$

dx.doi.org/10.1021/ic401180r | Inorg. Chem. XXXX, XXX, XXX−XXX

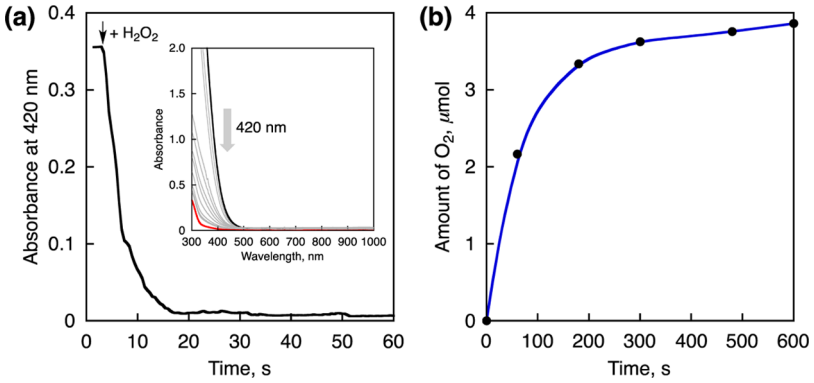

Figure 8. (a) Time course of the decay of CAN monitored at 420 nm in the reaction of H_2O_2 (2.0 mM) with CAN (4.0 mM) in the presence of HNO_3 (0.10 M) in an aqueous solution (2.0 mL). Inset shows the UV−vis spectral changes of the reaction solution. (b) Time course of O_2 evolution for H_2O_2 oxidation quantified by GC during the reaction of H_2O_2 (2.0 mM) with CAN (4.0 mM) in the presence of HNO_3 (0.10 M) in a nonbuffered aqueous solution (2.0 mL).

The subsequent oxidation of H_2O_2 would also be taking place in the iron metal center during the catalytic water oxidation. Thus, H_2O_2 cannot be involved in the rate-determining step for the four-electron oxidation of H_2O. The rate-determining step of the water oxidation by CAN may be the O−O bond formation in the oxidation of $[Fe^{IV}(BQEN)(O)(OH_2)]^{2+}$ by CAN (see Scheme 1). The oxidation of $[Fe^{IV}(BQEN)(O)(OH_2)]^{2+}$ by CAN may produce the Fe^{V} species as suggested by Costas, Fillol, and co-workers.[32] In this study, only $[Fe^{IV}(BQEN)(O)(OH_2)]^{2+}$ was observed during the water oxidation, although the formation of the Fe^{V} species cannot be excluded in the mechanism of water oxidation.

Light-Driven Water Oxidation by Iron Hydroxides Derived from 1. Under basic conditions, CAN is not a suitable oxidant for water oxidation, because hydrolysis of CAN occurs and reduces its oxidation power.[37] Thus, we examined the light-driven water oxidation under basic conditions using $[Ru(bpy)_3]^{2+}$ and $S_2O_8^{2-}$ as a photosensitizer and a sacrificial electron acceptor, respectively. The catalytic cycle of the light-driven water oxidation is shown in Scheme 2. Photoinduced

Scheme 2. Catalytic Cycle of Light-Driven Water Oxidation with $Na_2S_2O_8$ and $[Ru(bpy)_3]^{2+}$ Using an Iron-Based Catalyst

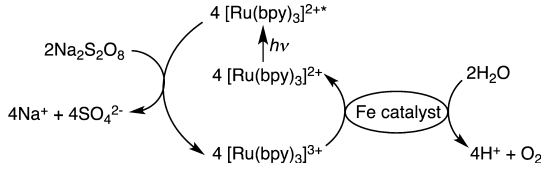

electron transfer from $[Ru(bpy)_3]^{2+}$* (where * denotes the excited state) to $S_2O_8^{2-}$ occurs to produce $[Ru(bpy)_3]^{3+}$, which can oxidize water in the presence of a WOC to evolve O_2. The light-driven water oxidation was performed in a borate buffer solution (0.10 M, 2.0 mL, initial pH 8.0, 8.5, or 9.0) containing **1** (5.0 μM), $Na_2S_2O_8$ (5.0 mM), and $[Ru(bpy)_3]SO_4$ (0.25 mM). The light-driven water oxidation reaction was started by irradiating the solution with a Xe lamp (500 W) through a transmitting glass filter (λ > 420 nm) with vigorous stirring at room temperature. Time courses of O_2 evolution at different initial pHs are shown in Figure 9a. The evolution of O_2 was not observed in the absence of **1** under the reaction conditions. The amount of O_2 obtained after 20 min photoirradiation at initial pH 9.0 (2.6 μmol, TON = 259) was larger than those at initial pH 8.5 (2.4 μmol, TON = 238) and 8.0 (0.67 μmol, TON = 67). The stoichiometric amount of O_2 evolution is 5.0 μmol in the present reaction systems based on the stoichiometry of eq 3, where $Na_2S_2O_8$ acts as a two-electron acceptor.[42]

$$2H_2O + 2Na_2S_2O_8 \rightarrow O_2 + 4H^+ + 4Na^+ + 4SO_4^{2-} \quad (3)$$

A high O_2 yield (52%) was obtained at initial pH 9.0. DLS measurements were performed to investigate the formation of nanoparticles in the reaction solution, since it has been reported that iron oxides formed during the reaction catalyze light-driven water oxidation by $S_2O_8^{2-}$.[33] Nanoparticles were detected by the DLS measurements as shown in Supporting Information, Figure S16. Figure 9b shows the time courses of average size of particles formed in the solution. Formation of nanoparticles even at the initial stage of photoirradiation indicates that nanoparticles derived from **1** act as a true catalyst in the light-driven water oxidation. In fact, the titration of sodium hydroxide to **1** monitored by UV−vis spectra demonstrated that the ligand of **1** was dissociated to release Fe^{2+} ions under basic condition (Supporting Information, Figure S17). As a result, nanoparticles derived from Fe^{2+} ions released from **1** by the ligand dissociation under the basic conditions act as the true catalyst in the light-driven water oxidation. When the concentration of **1** was increased to 1.0 mM, the ligand oxidation to CO_2 was also observed under the basic conditions (Supporting Information, Figure S18).

Nanoparticles also formed during the light-driven water oxidation with **2** at initial pH 9.0 (Supporting Information, Figure S19).

When the initial pH was 9.0, the final pH after the reaction slightly decreased to 8.6 (red line in Figure 9a) and the size of nanoparticles increased with the photoirradiation time to reach the size of 100 nm but slightly decreased as the pH decreased (red line in Figure 9b). When the initial pH was 8.5, the final pH decreased to 7.6 (blue line in Figure 9a), and the size of nanoparticles increased with the photoirradiation time. In the case of the initial pH 8.0, the final pH decreased significantly to 1.3 (green line in Figure 9a), and the nanoparticles formed initially disappeared at pH 1.3 (green line in Figure 9b). Under such an acidic condition, the O_2 yield decreased significantly as compared with those obtained under basic conditions.

When a phosphate buffer solution (50 mM, pH 8.0) was employed for the light-driven water oxidation, no O_2 evolution

dx.doi.org/10.1021/ic401180r | Inorg. Chem. XXXX, XXX, XXX−XXX

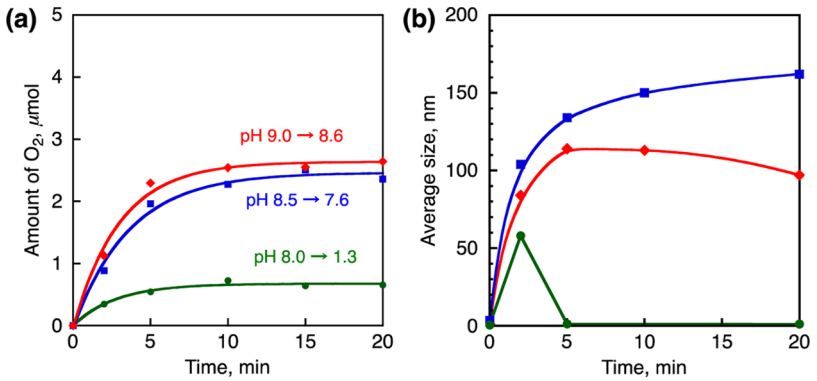

Figure 9. Time courses of O_2 evolution under photoirradiation ($\lambda > 420$ nm) of a borate buffer solution (0.10 M, 2.0 mL) containing $Na_2S_2O_8$ (5.0 mM), $[Ru(bpy)_3]SO_4$ (0.25 mM), and **1** (5.0 μM) at different initial pH conditions (green circles: pH 8.0, blue squares: pH 8.5, red rhombi: pH 9.0). (b) Time courses of average particle size formed in the photocatalytic reaction. See Supporting Information, Figure S13 for particle size distribution determined by dynamic light scattering (DLS) measurements.

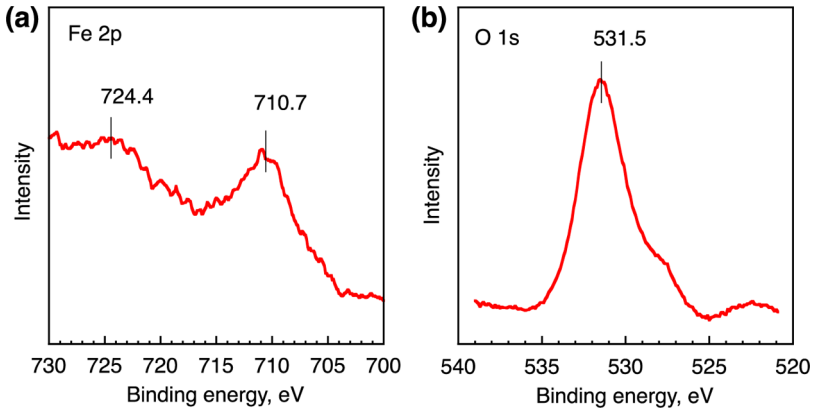

Figure 10. X-ray photoelectron spectra in the energy regions of (a) Fe 2p and (b) O 1s of the isolated particles formed in a borate buffer solution (100 mM, 2.0 mL) containing $Na_2S_2O_8$ (5.0 mM), $[Ru(bpy)_3]SO_4$ (0.25 mM), and **1** (1.0 mM). The binding energy of each element was corrected by the C 1s peak (284.6 eV) from the residual carbon.

Scheme 3. Iron Catalysts Derived from a Nonheme Iron Complex in Catalytic Water Oxidation at Different pHs

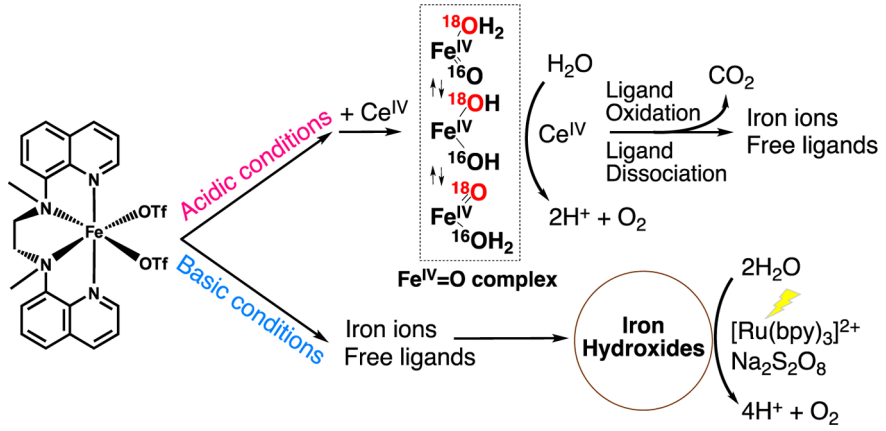

was observed by GC. In the phosphate buffer solution, dissolved Fe^{2+} ions were precipitated by phosphate anions.[33] The nanoparticles formed after the light-driven water oxidation by $S_2O_8^{2-}$ with **1** at the initial pH 9.0 were isolated, and they were found to be iron hydroxides by X-ray photoelectron spectroscopy (XPS) measurements (Figure 10) and transmission electron microscopy (TEM) measurements (Supporting Information, Figure S20), because higher binding energy of O 1s observed in Figure 10 indicates formation of hydroxide species rather than the oxide species.[43] Thus, the true catalyst in the light-driven water oxidation by $S_2O_8^{2-}$ is iron hydroxide nanoparticles derived from **1** at the initial stage of the reaction.

CONCLUSIONS

We have shown that the true catalysts that affect the water oxidation by iron complexes, **1** and **2**, are different in acidic and basic conditions, as shown in Scheme 3. The iron complexes act as homogeneous catalysts in the water oxidation by CAN under

dx.doi.org/10.1021/ic401180r | Inorg. Chem. XXXX, XXX, XXX−XXX

acidic conditions. The Fe^{IV}=O species formed by the two-electron oxidation of **1** and **2** by CAN in competition with the ligand dissociation under acidic conditions are involved in the catalytic water oxidation. The O−O bond formation may occur by the reaction of Fe^{IV}=O species with H_2O in the presence of 2 equiv of CAN or by the coupling of two Fe^{IV}=O species. The dissociated ligands are oxidized by CAN to yield CO_2, resulting in the decrease in the O_2 yield. In contrast to the homogeneous catalysis under acidic conditions, light-driven water oxidation using $[Ru(bpy)_3]^{2+}$ as a photosensitizer and $S_2O_8^{2-}$ as a sacrificial electron acceptor occurs under basic conditions, where **1** and **2** are converted to iron hydroxide nanoparticles that act as the true catalyst for the water oxidation. The iron complexes used here cannot act as efficient WOCs in their original forms, however, they provided an important mechanistic insight into actual form of molecular iron complexes in water oxidation. Although the intermediate on the surface of iron hydroxides in the photocatalytic system has yet to be identified, the present study provides valuable insights into the development of efficient WOCs using earth-abundant iron at different pHs.

■ ASSOCIATED CONTENT

Ⓢ Supporting Information

GC charts (Figure S1, S3, and S5), time course of O_2 evolution by manometry (Figure S2 and S6), ^{1}H NMR of the organic material (Figure S4), UV−vis spectra (Figures S7, S8, S11, S13, S15 and S17), DPV and CV (Figures S9 and S10), DLS measurements (Figures S12, S16, and S19), ESI-MS (Figure S14), time course of CO_2 evolution under basic conditions (Figure S18), and TEM images (Figure S20). This material is available free of charge via the Internet at http://pubs.acs.org.

■ AUTHOR INFORMATION

Corresponding Author

*E-mail: fukuzumi@chem.eng.osaka-u.ac.jp (S.F.), wwnam@ewha.ac.kr (W.N.), allobet@iciq.es (A.L.).

Author Contributions

‖These authors contributed equally to this work.

Notes

The authors declare no competing financial interest.

■ ACKNOWLEDGMENTS

This work at OU was supported by a Grant-in-Aid (Nos. 24350069 and 25600025) from the MEXT, Japan. The work at EWU was supported by NRF/MEST of Korea through CRI, GRL (2010-00353) and WCU (R31-2008-000-10010-0) Programs. A.L. thanks Generalitat de Catalunya and "la Caixa" Foundation for financial support. D.H. gratefully acknowledges support from JSPS by Grant-in-Aid for JSPS fellowship for young scientists. We acknowledge the Research Centre for Ultra-Precision Science & Technology for TEM measurements.

■ REFERENCES

(1) (a) Nocera, D. G. *Acc. Chem. Res.* **2012**, *45*, 767. (b) Lewis, N. S.; Nocera, D. G. *Proc. Natl. Acad. Sci. U. S. A.* **2006**, *103*, 15729.

(2) (a) Eisenberg, R.; Gray, H. B. *Inorg. Chem.* **2008**, *47*, 1697. (b) Gray, H. B. *Nat. Chem.* **2009**, *1*, 7. (c) Muckerman, J. T.; Polyansky, D. E.; Wada, T.; Tanaka, K.; Fujita, E. *Inorg. Chem.* **2008**, *47*, 1787.

(3) (a) Duan, L.; Tong, L.; Xu, Y.; Sun, L. *Energy Environ. Sci.* **2011**, *4*, 3296. (b) Artero, V.; Chavarot-Kerlidou, M.; Fontecave, M. *Angew. Chem., Int. Ed.* **2011**, *50*, 7238.

(4) (a) Fukuzumi, S. *Phys. Chem. Chem. Phys.* **2008**, *10*, 2283. (b) Fukuzumi, S.; Ohkubo, K. *J. Mater. Chem.* **2012**, *22*, 4575. (c) Fukuzumi, S.; Yamada, Y. *J. Mater. Chem.* **2012**, *22*, 24284.

(5) (a) Concepcion, J. J.; Jurss, J. W.; Brennaman, M. K.; Hoertz, P. G.; Patrocinio, A. O. T.; Murakami Iha, N. Y.; Templeton, J. L.; Meyer, T. J. *Acc. Chem. Res.* **2009**, *42*, 1954. (b) Magnuson, A.; Anderlund, M.; Johansson, O.; Lindblad, P.; Lomoth, R.; Polivka, T.; Ott, S.; Stensjo, K.; Styring, S.; Sundstrom, V.; Hammarstrom, L. *Acc. Chem. Res.* **2009**, *42*, 1899.

(6) Fukuzumi, S.; Yamada, Y.; Suenobu, T.; Ohkubo, K.; Kotani, H. *Energy Environ. Sci.* **2011**, *4*, 2754.

(7) (a) Hetterscheid, D. G. H.; Reek, J. N. H. *Angew. Chem., Int. Ed.* **2012**, *51*, 9740. (b) Cao, R.; Lai, W.; Du, P. *Energy Environ. Sci.* **2012**, *5*, 8134. (c) Sala, X.; Romero, I.; Rodriguez, M.; Escriche, L.; Llobet, A. *Angew. Chem., Int. Ed.* **2009**, *48*, 2842.

(8) (a) Hurst, J. K.; Cape, J. L.; Clark, A. E.; Das, S.; Qin, C. Y. *Inorg. Chem.* **2008**, *47*, 1753. (b) Deng, Z. P.; Tseng, H. W.; Zong, R. F.; Wang, D.; Thummel, R. *Inorg. Chem.* **2008**, *47*, 1835.

(9) (a) Gersten, S. W.; Samuels, G. J.; Meyer, T. J. *J. Am. Chem. Soc.* **1982**, *104*, 4029. (b) Lebeau, E. L.; Adeyemi, S. A.; Meyer, T. J. *Inorg. Chem.* **1998**, *37*, 6476. (c) Concepcion, J. J.; Jurss, J. W.; Norris, M. R.; Chen, Z. F.; Templeton, J. L.; Meyer, T. J. *Inorg. Chem.* **2010**, *49*, 1277.

(10) (a) Harriman, A.; Pickering, I. J.; Thomas, J. M.; Christensen, P. A. *J. Chem. Soc., Faraday Trans. I* **1988**, *84*, 2795. (b) Jiao, F.; Frei, H. *Energy Environ. Sci.* **2010**, *3*, 1018. (c) Morris, N. D.; Mallouk, T. E. *J. Am. Chem. Soc.* **2002**, *124*, 11114.

(11) (a) Murakami, M.; Hong, D.; Suenobu, T.; Yamaguchi, S.; Ogura, T.; Fukuzumi, S. *J. Am. Chem. Soc.* **2011**, *133*, 11605. (b) Polyansky, D. E.; Muckerman, J. T.; Rochford, J.; Zong, R.; Thummel, R. P.; Fujita, E. *J. Am. Chem. Soc.* **2011**, *133*, 14649. (c) Boyer, J. L.; Polyansky, D. E.; Szalda, D. J.; Zong, R.; Thummel, R. P.; Fujita, E. *Angew. Chem., Int. Ed.* **2011**, *50*, 12600. (d) Kimoto, A.; Yamauchi, K.; Yoshida, M.; Masaoka, S.; Sakai, K. *Chem. Commun.* **2012**, *48*, 239. (e) Kärkäs, M. D.; Åkermark, T.; Johnston, E. V.; Karim, S. R.; Laine, T. M.; Lee, B.-L.; Åkermark, T.; Privalov, T.; Åkermark, B. *Angew. Chem., Int. Ed.* **2012**, *51*, 11589.

(12) (a) Mola, J.; Mas-Marza, E.; Sala, X.; Romero, I.; Rodriguez, M.; Vinas, C.; Parella, T.; Llobet, A. *Angew. Chem., Int. Ed.* **2008**, *47*, 5830. (b) Bozoglian, F.; Romain, S.; Ertem, M. Z.; Todorova, T. K.; Sens, C.; Mola, J.; Rodriguez, M.; Romero, I.; Benet-Buchholz, J.; Fontrodona, X.; Cramer, C. J.; Gagliardi, L.; Llobet, A. *J. Am. Chem. Soc.* **2009**, *131*, 15176.

(13) (a) Geletii, Y. V.; Botar, B.; Koegerler, P.; Hillesheim, D. A.; Musaev, D. G.; Hill, C. L. *Angew. Chem., Int. Ed.* **2008**, *47*, 3896. (b) Geletii, Y. V.; Besson, C.; Hou, Y.; Yin, Q. S.; Musaev, D. G.; Quinonero, D.; Cao, R.; Hardcastle, K. I.; Proust, A.; Kogerler, P.; Hill, C. L. *J. Am. Chem. Soc.* **2009**, *131*, 17360. (c) Sartorel, A.; Carraro, M.; Scorrano, G.; De Zorzi, R.; Geremia, S.; McDaniel, N. D.; Bernhard, S.; Bonchio, M. *J. Am. Chem. Soc.* **2008**, *130*, 5006.

(14) (a) Duan, L.; Bozoglian, F.; Mandal, S.; Stewart, B.; Privalov, T.; Llobet, A.; Sun, L. *Nat. Chem.* **2012**, *4*, 418. (b) Jiang, Y.; Li, F.; Zhang, B.; Li, X.; Wang, X.; Huang, F.; Sun, L. *Angew. Chem., Int. Ed.* **2013**, *52*, 3398. (c) Duan, L. L.; Xu, Y. H.; Zhang, P.; Wang, M.; Sun, L. C. *Inorg. Chem.* **2010**, *49*, 209. (d) Wang, L.; Duan, L.; Stewart, B.; Pu, M.; Liu, J.; Privalov, T.; Sun, L. *J. Am. Chem. Soc.* **2012**, *134*, 18868. (e) Xu, Y.; Fischer, A.; Duan, L.; Tong, L.; Gabrielsson, E.; Åkermark, B.; Sun, L. *Angew. Chem., Int. Ed.* **2010**, *49*, 8934.

(15) (a) Kaveevivitchai, N.; Chitta, R.; Zong, R.; El Ojaimi, M.; Thummel, R. P. *J. Am. Chem. Soc.* **2012**, *134*, 10721. (b) Natali, M.; Orlandi, M.; Berardi, S.; Campagna, S.; Bonchio, M.; Sartorel, A.; Scandola, F. *Inorg. Chem.* **2012**, *51*, 7324.

(16) (a) Francas, L.; Sala, X.; Escudero-Adan, E.; Benet-Buchholz, J.; Escriche, L.; Llobet, A. *Inorg. Chem.* **2011**, *50*, 2771. (b) Radaram, B.; Ivie, J. A.; Singh, W. M.; Grudzien, R. M.; Reibenspies, J. H.; Webster, C. E.; Zhao, X. *Inorg. Chem.* **2011**, *50*, 10564.

(17) (a) Morris, N. D.; Suzuki, M.; Mallouk, T. E. *J. Phys. Chem. A* **2004**, *108*, 9115. (b) Yagi, M.; Tomita, E.; Sakita, S.; Kuwabara, T.; Nagai, K. *J. Phys. Chem. B* **2005**, *109*, 21489. (c) Hoertz, P. G.; Kim, Y. I.; Youngblood, W. J.; Mallouk, T. E. *J. Phys. Chem. B* **2007**, *111*, 6845.
(18) (a) McDaniel, N. D.; Coughlin, F. J.; Tinker, L. L.; Bernhard, S. *J. Am. Chem. Soc.* **2008**, *130*, 210. (b) Blakemore, J. D.; Schley, N. D.; Balcells, D.; Hull, J. F.; Olack, G. W.; Incarvito, C. D.; Eisenstein, O.; Brudvig, G. W.; Crabtree, R. H. *J. Am. Chem. Soc.* **2010**, *132*, 16017. (c) Lalrempuia, R.; McDaniel, N. D.; Muller-Bunz, H.; Bernhard, S.; Albrecht, M. *Angew. Chem., Int. Ed.* **2010**, *49*, 9765.
(19) (a) Savini, A.; Bellachioma, G.; Ciancaleoni, G.; Zuccaccia, C.; Zuccaccia, D.; Macchioni, A. *Chem. Commun.* **2010**, *46*, 9218. (b) Savini, A.; Bellachioma, G.; Bolano, S.; Rocchigiani, L.; Zuccaccia, C.; Zuccaccia, D.; Macchioni, A. *ChemSusChem* **2012**, *5*, 1415. (c) Wang, C.; Wang, J.-L.; Lin, W. *J. Am. Chem. Soc.* **2012**, *134*, 19895.
(20) (a) Hong, D.; Murakami, M.; Yamada, Y.; Fukuzumi, S. *Energy Environ. Sci.* **2012**, *5*, 5708. (b) Hintermair, U.; Hashmi, S. M.; Elimelech, M.; Crabtree, R. H. *J. Am. Chem. Soc.* **2012**, *134*, 9785. (c) Zuccaccia, C.; Bellachioma, G.; Bolano, S.; Rocchigiani, L.; Savini, A.; Macchioni, A. *Eur. J. Inorg. Chem.* **2012**, 1462. (d) Grotjahn, D. B.; Brown, D. B.; Martin, J. K.; Marelius, D. C.; Abadjian, M.-C.; Tran, H. N.; Kalyuzhny, G.; Vecchio, K. S.; Specht, Z. G.; Cortes-Llamas, S. A.; Miranda-Soto, V.; van Niekerk, C.; Moore, C. E.; Rheingold, A. L. *J. Am. Chem. Soc.* **2011**, *133*, 19024.
(21) (a) Kanan, M. W.; Nocera, D. G. *Science* **2008**, *321*, 1072. (b) Stracke, J. J.; Finke, R. G. *J. Am. Chem. Soc.* **2011**, *133*, 14872. (c) Gerken, J. B.; McAlpin, J. G.; Chen, J. Y. C.; Rigsby, M. L.; Casey, W. H.; Britt, R. D.; Stahl, S. S. *J. Am. Chem. Soc.* **2011**, *133*, 14431. (d) McAlpin, J. G.; Surendranath, Y.; Dinca, M.; Stich, T. A.; Stoian, S. A.; Casey, W. H.; Nocera, D. G.; Britt, R. D. *J. Am. Chem. Soc.* **2010**, *132*, 6882.
(22) (a) Yin, Q. S.; Tan, J. M.; Besson, C.; Geletii, Y. V.; Musaev, D. G.; Kuznetsov, A. E.; Luo, Z.; Hardcastle, K. I.; Hill, C. L. *Science* **2010**, *328*, 342. (b) Natali, M.; Berardi, S.; Sartorel, A.; Bonchio, M.; Campagna, S.; Scandola, F. *Chem. Commun.* **2012**, *48*, 8808. (c) Huang, Z.; Luo, Z.; Geletii, Y. V.; Vickers, J. W.; Yin, Q.; Wu, D.; Hou, Y.; Ding, Y.; Song, J.; Musaev, D. G.; Hill, C. L.; Lian, T. *J. Am. Chem. Soc.* **2011**, *133*, 2068. (d) Tanaka, S.; Annaka, M.; Sakai, K. *Chem. Commun.* **2012**, *48*, 1653.
(23) (a) Jiao, F.; Frei, H. *Angew. Chem., Int. Ed.* **2009**, *48*, 1841. (b) Wee, T.-L.; Sherman, B. D.; Gust, D.; Moore, A. L.; Moore, T. A.; Liu, Y.; Scaiano, J. C. *J. Am. Chem. Soc.* **2011**, *133*, 16742.
(24) Hong, D.; Jung, J.; Park, J.; Yamada, Y.; Suenobu, T.; Lee, Y.-M.; Nam, W.; Fukuzumi, S. *Energy Environ. Sci.* **2012**, *5*, 7606.
(25) (a) Barnett, S. M.; Goldberg, K. I.; Mayer, J. M. *Nat. Chem.* **2012**, *4*, 498. (b) Zhang, M.-T.; Chen, Z.; Kang, P.; Meyer, T. J. *J. Am. Chem. Soc.* **2013**, *135*, 2048.
(26) (a) Yagi, M.; Narita, K. *J. Am. Chem. Soc.* **2004**, *126*, 8084. (b) Jiao, F.; Frei, H. *Chem. Commun.* **2010**, *46*, 2920. (c) Najafpour, M. M. *Chem. Commun.* **2011**, *47*, 11724.
(27) (a) Gao, Y.; Crabtree, R. H.; Brudvig, G. W. *Inorg. Chem.* **2012**, *51*, 4043. (b) Dismukes, G. C.; Brimblecombe, R.; Kolling, D. R. J.; Bond, A. M.; Swiegers, G. F.; Spiccia, L. *Inorg. Chem.* **2009**, *48*, 7269.
(28) Najafpour, M. M.; Moghaddam, A. N. *Dalton Trans.* **2012**, *41*, 10292.
(29) (a) Kim, T. V.; Elizarova, G. L.; Parmon, V. N. *React. Kinet. Catal. Lett.* **1984**, *26*, 57. (b) Hong, D.; Yamada, Y.; Nagatomi, T.; Takai, Y.; Fukuzumi, S. *J. Am. Chem. Soc.* **2012**, *134*, 19572. (c) Ellis, W. C.; McDaniel, N. D.; Bernhard, S.; Collins, T. J. *J. Am. Chem. Soc.* **2010**, *132*, 10990. (d) Kundu, S.; Matito, E.; Walleck, S.; Pfaff, F. F.; Heims, F.; Rábay, B.; Luis, J. M.; Company, A.; Braun, B.; Glaser, T.; Ray, K. *Chem.—Eur. J.* **2012**, *18*, 2787. (e) Hoffert, W. A.; Mock, M. T.; Appel, A. M.; Yang, J. Y. *Eur. J. Inorg. Chem.* 2013, in press. DOI: 10.1002/ejic.201201499. (f) Codolà, Z.; Garcia-Bosch, I.; Acuña-Parés, F.; Prat, I.; Luis, J. M.; Costas, M.; Lloret-Fillol, J. *Chem.—Eur. J.* **2013**, *19*, 8042.
(30) (a) Sun, C.-L.; Li, B.-J.; Shi, Z.-J. *Chem. Rev.* **2011**, *111*, 1293. (b) Chow, T. W.-S.; Chen, G.-Q.; Liu, Y.; Zhou, C.-Y.; Che, C.-M. *Pure Appl. Chem.* **2012**, *84*, 1685. (c) Talsi, E. P.; Bryliakov, K. P. *Coord. Chem. Rev.* **2012**, *256*, 1418. (d) Sun, X.; Li, J.; Huang, X.; Sun, C. *Curr. Inorg. Chem.* **2012**, *2*, 64.
(31) (a) Allpress, C. J.; Grubel, K.; Szajna-Fuller, E.; Arif, A. M.; Berreau, L. M. *J. Am. Chem. Soc.* **2013**, *135*, 659. (b) Bugg, T. D. H.; Ramaswamy, S. *Curr. Opin. Chem. Biol.* **2008**, *12*, 134. (c) Kim, Y. J.; Feng, X.; Lippard, S. J. *Inorg. Chem.* **2007**, *46*, 6099.
(32) Fillol, J. L.; Codolà, Z.; Garcia-Bosch, I.; Gómez, L.; Pla, J. J.; Costas, M. *Nat. Chem.* **2011**, *3*, 807.
(33) Chen, G.; Chen, L.; Ng, S.-M.; Man, W.-L.; Lau, T.-C. *Angew. Chem., Int. Ed.* **2013**, *52*, 1789.
(34) (a) Artero, V.; Fonteacave, M. *Chem. Soc. Rev.* **2013**, *42*, 2338. (b) Fukuzumi, S.; Hong, D. *Eur. J. Inorg. Chem.* in press. DOI: 10.1002/ejic.201300684.
(35) Hagen, K. S. *Inorg. Chem.* **2000**, *39*, 5867.
(36) (a) England, J.; Britovsek, G. J. P.; Rabadia, N.; White, A. J. P. *Inorg. Chem.* **2007**, *46*, 3752. (b) Hong, S.; Lee, Y.-M.; Cho, K.-B.; Sundaravel, K.; Cho, J.; Kim, M. J.; Shin, W.; Nam, W. *J. Am. Chem. Soc.* **2011**, *133*, 11876.
(37) Wadsworth, E.; Duke, F. R.; Goetz, C. A. *Anal. Chem.* **1957**, *29*, 1824.
(38) (a) Baalousha, M.; Manciulea, A.; Cumberland, S.; Kendall, K.; Lead, J. R. *Environ. Toxicol. Chem.* **2008**, *27*, 1875. (b) Mandel, K.; Szczerba, W.; Thünemann, A. F.; Riesemeier, H.; Girod, M.; Sextl, G. *J. Nanopart. Res.* **2012**, *14*, 1066.
(39) Lee, Y.-M.; Dhuri, S. N.; Sawant, S. C.; Cho, J.; Kubo, M.; Ogura, T.; Fukuzumi, S.; Nam, W. *Angew. Chem., Int. Ed.* **2009**, *48*, 1803.
(40) Yoon, J.; Wilson, S. A.; Jang, Y. K.; Seo, M. S.; Nehru, K.; Hedman, B.; Hodgson, K. O.; Bill, E.; Solomon, E. I.; Nam, W. *Angew. Chem., Int. Ed.* **2009**, *48*, 1257.
(41) Measurements of ESI-MS spectra required the presence of MeCN. $[Fe^{III}(BQEN)(^{16}OH)(OTf)]^+$ and $[Fe^{III}(BQEN)(^{18}OH)(OTf)]^+$ were detected by ESI-MS spectroscopy in the reaction of **1** (1.0 mM) with CAN (2.0 mM) in $H_2{}^{16}O$/MeCN (1:4 v/v) and $H_2{}^{18}O$/MeCN (1:4 v/v), respectively (Supporting Information, Figure S14). The formation of $[Fe^{IV}(BQEN)(O)]^{2+}$ by CAN may be unstable under the ESI-MS measurements.
(42) Kaledin, A. L.; Huang, Z.; Geletii, Y. V.; Lian, T.; Hill, C. L.; Musaev, D. G. *J. Phys. Chem. A* **2010**, *114*, 73.
(43) (a) Yamada, Y.; Yano, K.; Xu, Q. A.; Fukuzumi, S. *J. Phys. Chem. C* **2010**, *114*, 16456. (b) Mcintyre, N. S.; Zetaruk, D. G. *Anal. Chem.* **1977**, *49*, 1521. (c) Mathew, T.; Shiju, N. R.; Sreekumar, K.; Rao, B. S.; Gopinath, C. S. *J. Catal.* **2002**, *210*, 405.